Technical Report 32-1403

Cold-Flow Experimental Investigation and Analysis of Two Sources of Nozzle Thrust Misalignment

L. D. Strand
Jet Propulsion Laboratory
M. W. Dowdy
The Martin Company

JET PROPULSION LABORATORY
CALIFORNIA INSTITUTE OF TECHNOLOGY
PASADENA, CALIFORNIA

September 15, 1969

NATIONAL AERONAUTICS AND SPACE ADMINISTRATION

Technical Report 32-1403

Cold-Flow Experimental Investigation and Analysis of Two Sources of Nozzle Thrust Misalignment

L. D. Strand
Jet Propulsion Laboratory
M. W. Dowdy
The Martin Company

JET PROPULSION LABORATORY
CALIFORNIA INSTITUTE OF TECHNOLOGY
PASADENA, CALIFORNIA

September 15, 1969

Prepared Under Contract No. NAS 7-100
National Aeronautics and Space Administration

Preface

The work described in this report was performed by the Propulsion Division of the Jet Propulsion Laboratory.

Acknowledgment

The contributions of Messrs. J. G. Herrera and R. B. Morrow, Aerodynamic Facilities project engineer and technician, respectively, for the test program, and Mr. L. W. Schmele, for performing the computer program modifications and asymmetric-nozzle parametric calculations, are gratefully acknowledged.

Contents

Table

Contents (contd)

Figures

Contents (contd)

Figures (contd)

Abstract

A research program was performed to investigate the effects of nozzle surface irregularities and throat asymmetry on the rocket-nozzle thrust vector. The program consisted of experimental tests, conducted in a three-dimensional gas-flow test facility, measuring the surface pressure distribution of three test-nozzle configurations, an axisymmetric nozzle, the symmetric nozzle with a protrusion to the flow located in the conical expansion region, and a nozzle with an asymmetrical throat; calculation of the nozzle side forces by summation of the test-pressure data over the nozzle surfaces; comparison of the test data with the results of several simplified flow-field analyses; and the carrying out of a two-dimensional asymmetric nozzle parametric study. From the test results, it was concluded that nozzle surface irregularities and throat asymmetry can produce measurable and possibly significant side forces. Guided by the results of the analyses performed, recommendations are made for application of the program results to actual rocket-nozzle conditions.

Cold-Flow Experimental Investigation and Analysis of Two Sources of Nozzle Thrust Misalignment

I. Introduction

A research program was formulated to investigate two areas of rocket-nozzle aerodynamics that have been relatively neglected to date: the effects, if any, of (1) nozzle surface irregularities and (2) throat asymmetry upon the position of the nozzle thrust vector. Such irregularities and asymmetry can result from the delamination or erosion of nozzle ablative materials during rocket firing. The program goals were (1) to determine whether an exaggerated asymmetry in the nozzle-throat cross section displaced the thrust vector and, if so, to what magnitude, and (2) to extend flat-plate protrusion data to nozzle flow to determine the extent to which a protrusion to the flow in the nozzle expansion region displaces the thrust vector.

II. Test Program

A. Auxiliary Flow Channel

The experimental tests were conducted in a three-dimensional gas-flow test facility, designated the auxiliary flow channel. A comprehensive description of the channel and its performance characteristics is given in Ref. 1; only a brief summary is given herein. The flow channel consists of a gas line tapped off of the JPL hypersonic 21-in. wind tunnel downstream from the heated-air supply section and upstream from the inlet valve to the test section. The line exhausts into the tunnel diffuser, bypassing the wind-tunnel test section. The test assembly (Fig. 1) consists of a plenum chamber to straighten and stabilize the flow, a reducer section, the nozzle in use, an expansion joint to allow for nozzle removal, and a spacer section to accommodate test nozzles of increased length.

The air-supply capabilities of the auxiliary flow channel are essentially the same as those of the hypersonic wind tunnel (neglecting losses in the inlet line): approximately 660 psia maximum supply pressure and 10 lb/s maximum air-flow rate. The compressors can maintain a diffuser-backpressure-to-supply-pressure ratio of 0.002. By utilizing the hypersonic heater, the supply temperature can be varied and controlled from 90 to 1350°F.

B. Test Nozzles

Two steel nozzles of equal throat area (1.0 $in.^2$), with an expansion ratio of 18:1 and an overall length of

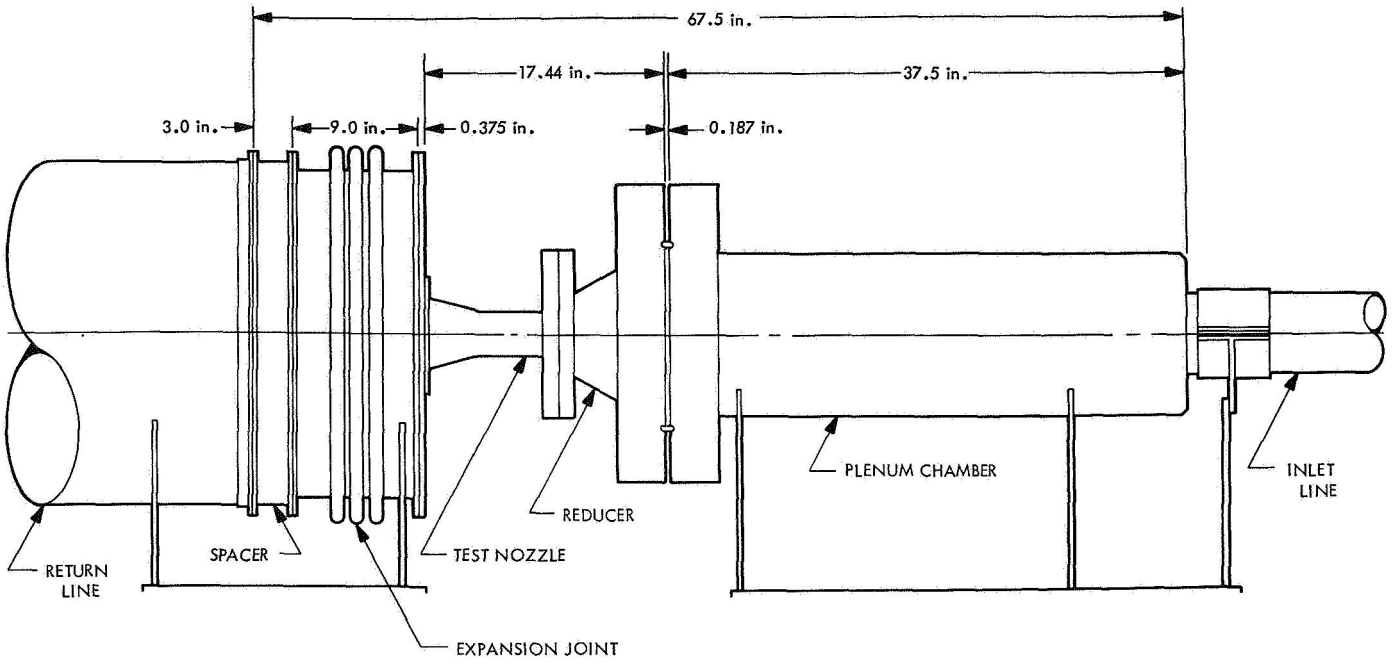

Fig. 1. Gas-flow nozzle test assembly

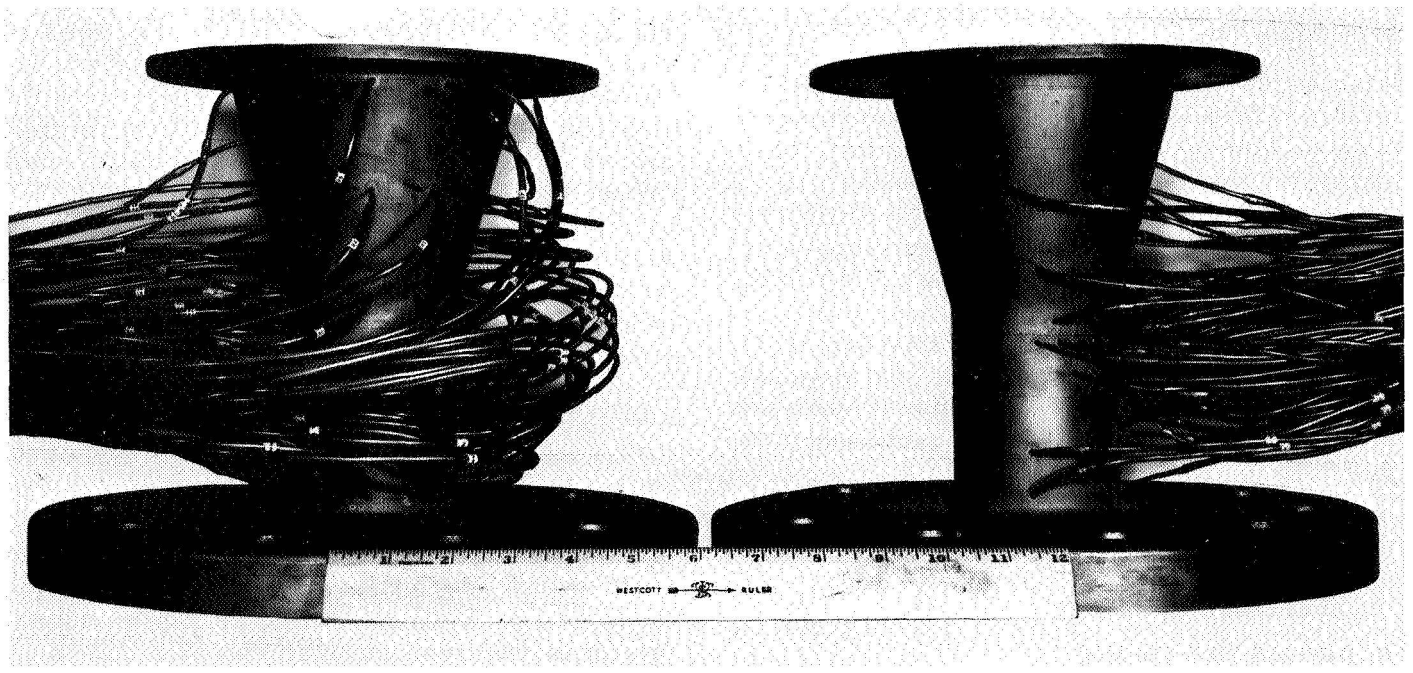

Fig. 2. Test nozzles

9.56 in., were fabricated as part of the test assembly (Fig. 2). The inner surfaces of the nozzles were nickel- and chrome-plated to resist corrosion. The nozzles were instrumented with static-pressure orifices on the surfaces of both the nozzle throat section and the expansion cone, allowing the wall-pressure distribution to be determined. By integrating the pressure distribution over the nozzle surface, an analytical approximation of the force imbalance normal to the nozzle axis could be obtained.

Both nozzles were conical, with 30-deg entrance and 15-deg exit cones. One nozzle was axisymmetric, with a throat radius of curvature of 2.82 in. and a throat radius of 0.571 in., giving a radius-of-curvature-to-throat-radius ratio r_c/r_t of 4.91. The exit diameter was 4.830 in. To determine the effect of a nozzle protrusion, two removable inserts were made for the nozzle, both mounted in the nozzle wall 1.90 in. aft of the nozzle throat. The surface of one insert fit flush with the nozzle surface. The second insert had a 0.125-in. square protrusion that extended 0.150 in. above the surface of the nozzle. The nozzle internal surface had 85 static-pressure orifices, fabricated of 0.0465- and 0.061-in. inside diameters (ID) stainless-steel tubing. Figure 3 is a cross-sectional sketch along the pressure-orifice centerline showing the axial spacing of the orifice positions. Figure 4 is a flattened-out representation of the pressure-orifice spacing about the orifice centerline. The protrusion, mounted in place, is shown in a view looking upstream from the nozzle exit (Fig. 5).

The second test nozzle was fabricated with a known throat-region asymmetry. The throat cross section was composed of half an ellipse and half a circle. Figure 6 is a sketch of the nozzle cross section along the major axis of the ellipse. The radius of the circle at the design geometric throat was 0.526 in. The elliptical portion had a fixed major axis of 0.705 in. The minor axis of the ellipse equaled the radius of the circular portion, resulting in a smooth, continuous surface. The area centroid

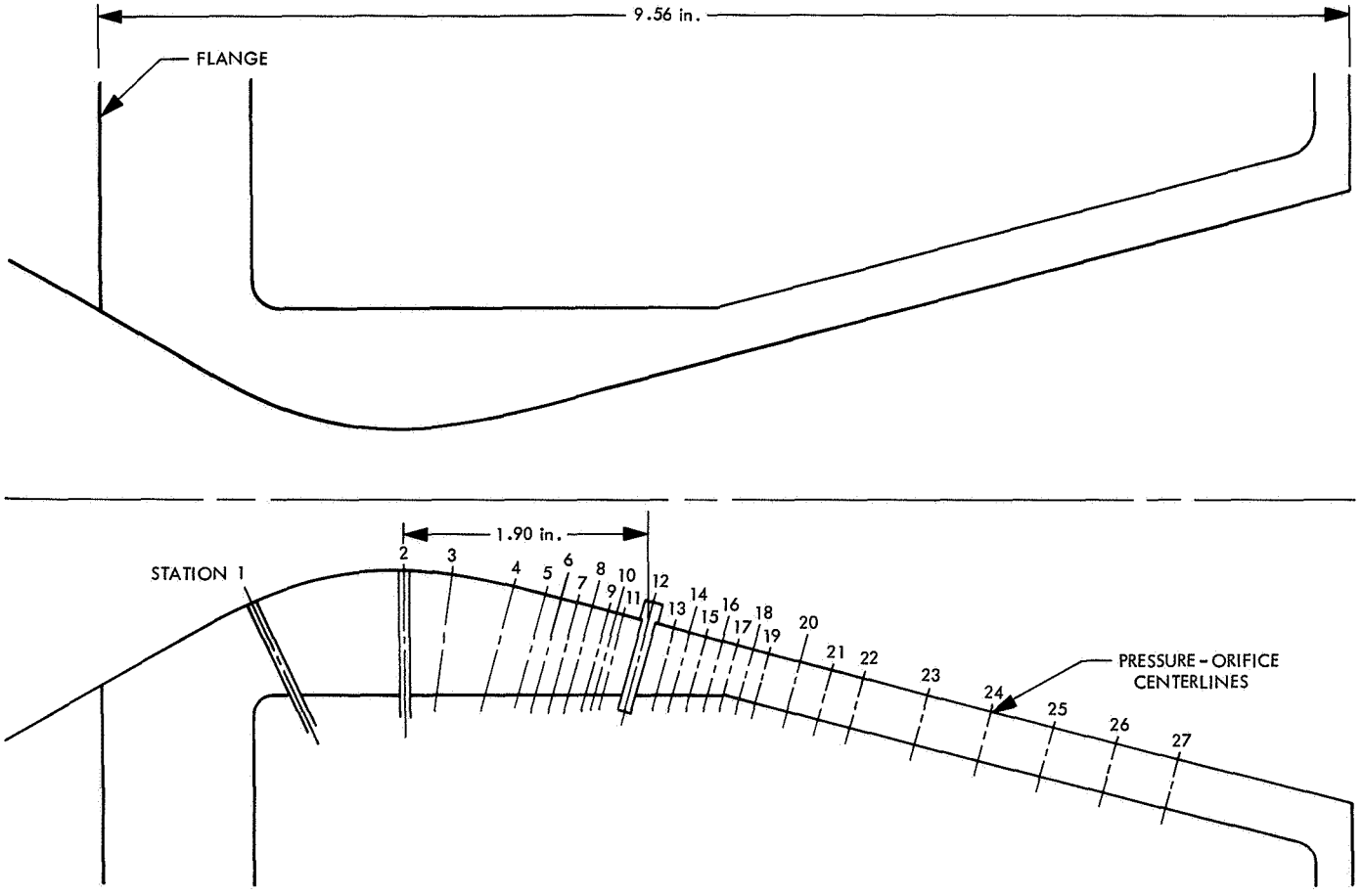

Fig. 3. Symmetric nozzle cross section

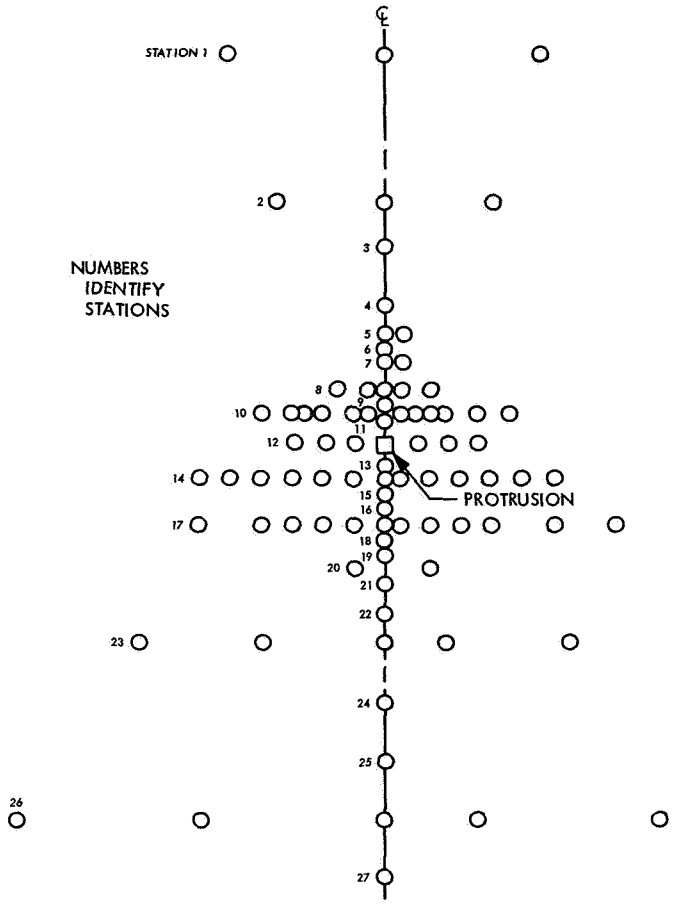

Fig. 4. Symmetric nozzle in-the-flat pressure-orifice spacing

at the throat was biased 0.072 in. from the nozzle centerline. At the nozzle axial positions of transition to symmetry on either side of the throat, the major and minor axes of the ellipse became equal. The symmetrical throat-region radii of curvature were 2.77 in. fore and 3.35 in. aft. This nozzle inner surface contained 100 static-pressure orifices, 0.061-in.-ID tubing being used exclusively. The axial spacing of the 14 pressure-orifice stations is shown in Fig. 6. One of the four cross-sectional orifice configurations shown in Fig. 7 was used at each station.

C. Instrumentation

Static-pressure measurements were made with an electromechanical multipressure measuring system (MPMS). The MPMS is composed of 10 modules, each module containing 12 ports. A pressure transducer located in each module scans all 12 ports upon command, measuring the pressure of each port. The module scanning time was approximately 20 s. For this test, the MPMS was modified to withstand pressures greater than 600 psia. Each 12-port module of the system was connected to 11 pressure lines and 1 reference pressure. Figure 8 shows the symmetric nozzle mounted in the test assembly with its pressure-orifice lines connected to the MPMS.

Eight modules were used to measure the 85 static pressures plus the plenum chamber pressure. The wide range of pressures was measured with 50-, 100-, 250-, and 1000-psia pressure transducers in the modules, with measurement sensitivities of 0.1% (or better) of the transducer full-scale values. Reference pressures of 14.7, 100, and 200 psia were used throughout the test. Nine modules were used for the 100-port asymmetric nozzle. The data from the transducers were converted by a computer to pressure values in torr and to several pressure ratios, using the transducer calibration inputs. The plenum-chamber air temperature was continuously monitored with a Chromel–Alumel thermocouple at a reference temperature of 150°F.

D. Test Procedure

The tests were grouped into three series. The first series of tests was run with the symmetrical nozzle and no flow disturbance, the second with the symmetrical nozzle with flow disturbance, and the third with the asymmetric nozzle. The functions of the first tests were to check the flow uniformity and instrumentation accuracy of the test system and to provide a baseline for interpreting the results of the protrusion tests. Assurance of uniform flow with no apparent vortices was obtained by rotating the nozzle in the test assembly approximately 90 deg from its normal position and repeating a few of the test runs. No significant changes in the wall static pressures were measured.

Each series of tests consisted of a run at each of seven supply pressures: 100, 200, 300, 400, 450, 500, and 600 psia. The procedure for each run was to establish the required plenum pressure, care being taken to allow the pressure to stabilize. The MPMS was then energized, and four scans of the nozzle static-pressure orifices were taken, giving four sets of pressure data. By means of controls, the tunnel compressor plant was then adjusted to supply air at each of the remaining required plenum pressures. The supply air temperature was raised to only a high enough level (approximately 140°F) to ensure against air liquefaction in the nozzle expansion region. The air temperature was controlled by varying the cooling of the compressor stage.

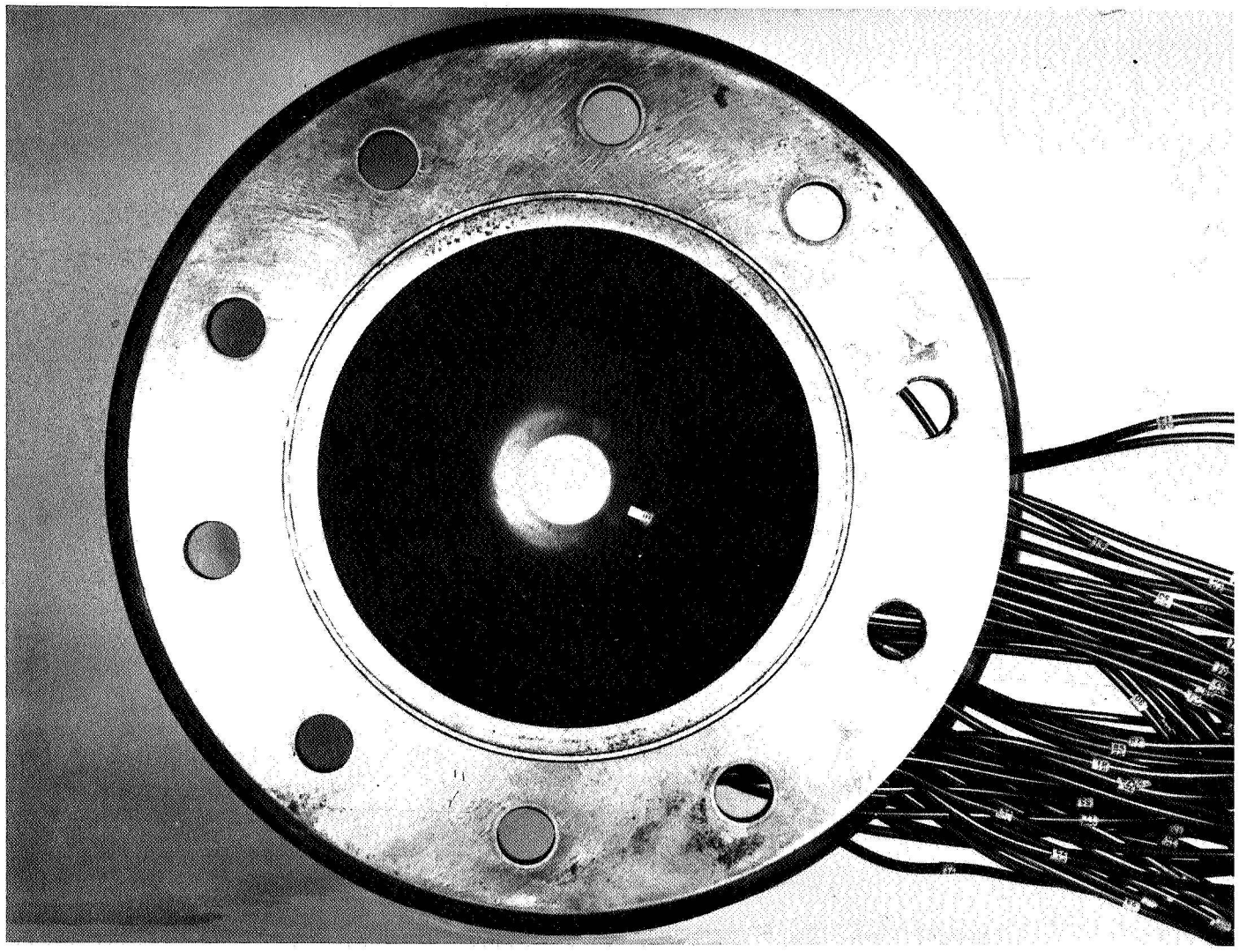

Fig. 5. Symmetric nozzle, aft view

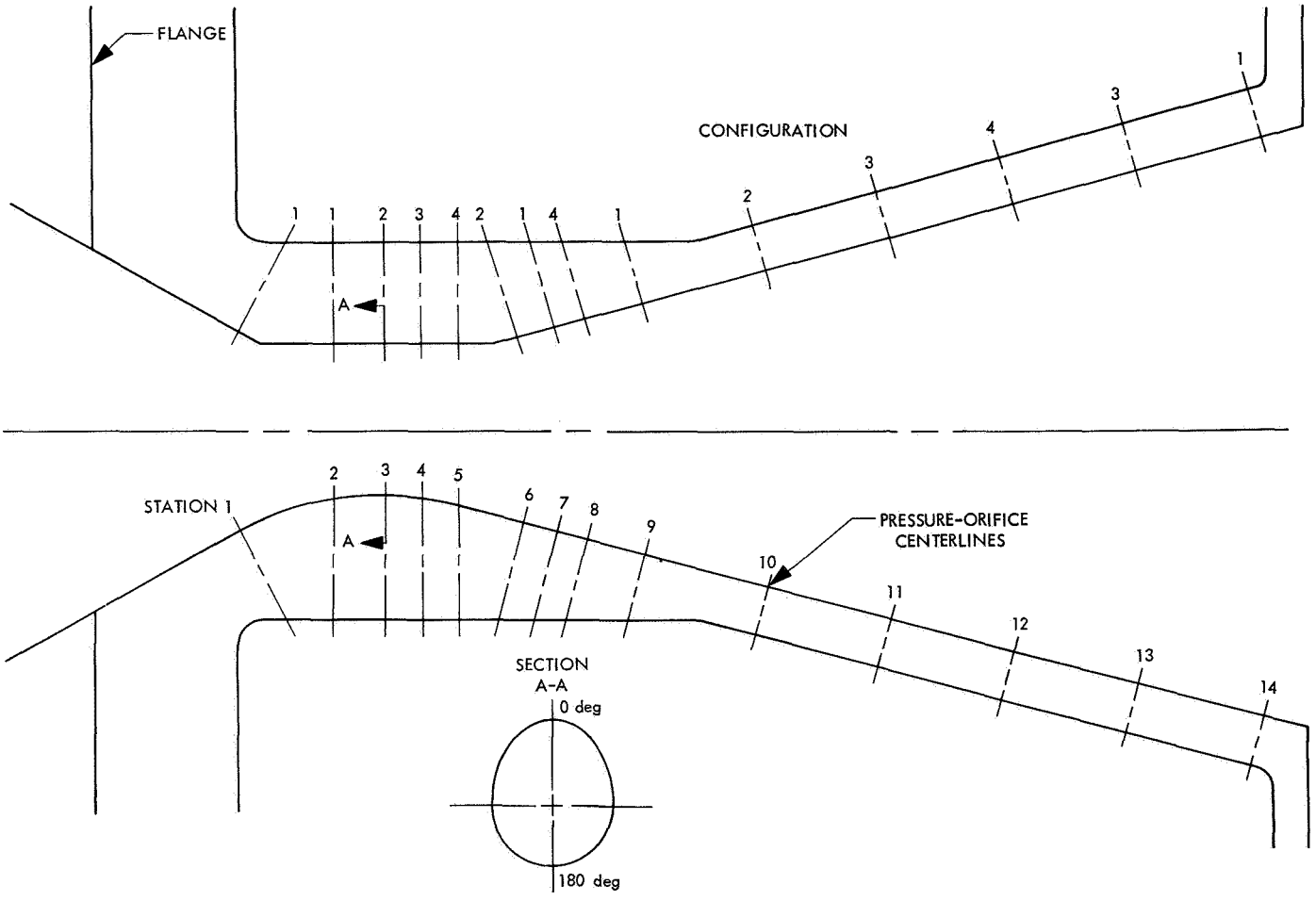

Fig. 6. Asymmetric nozzle cross section

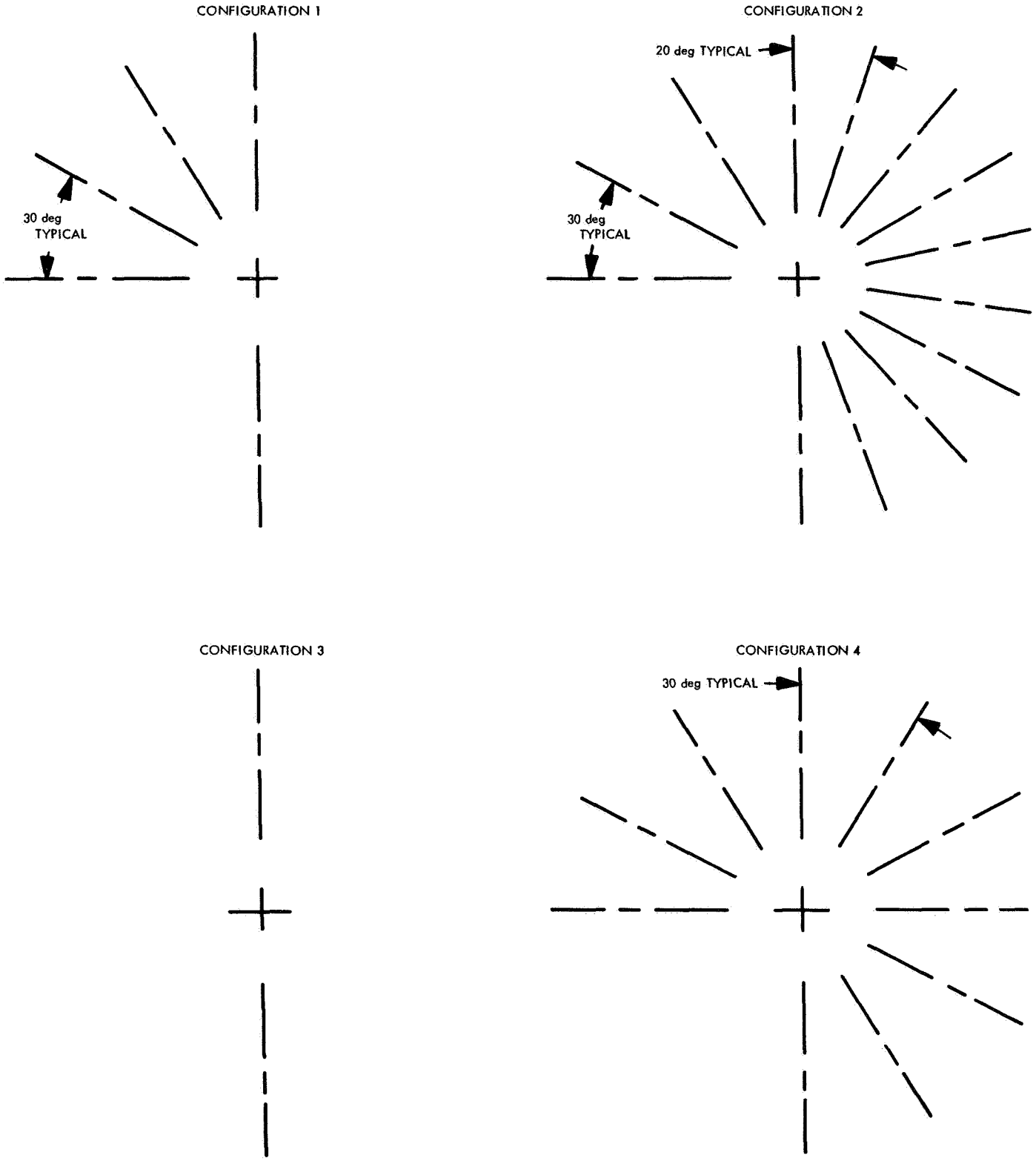

Fig. 7. Axial-station pressure-orifice configurations, asymmetric nozzle

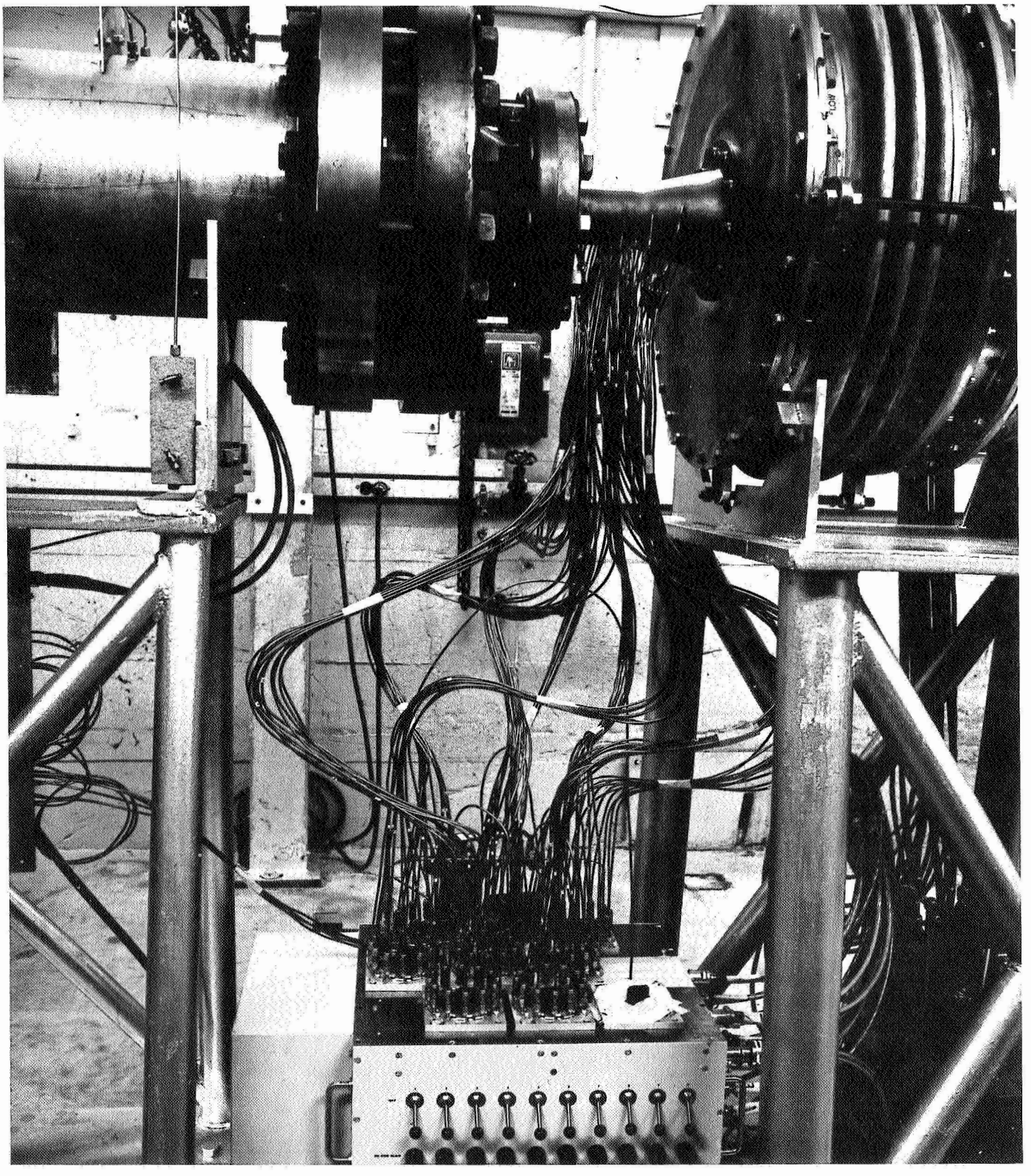

Fig. 8. Test assembly multipressure measuring system

III. Experimental Results

A. Symmetric Nozzle

The symmetric-nozzle tests had to be run twice. Because of improper bonding of the chrome plating to the symmetric-nozzle surface, the plating became damaged when the protrusion for the second series of tests was installed in the nozzle. Subsequently, all of the plating could be peeled off, and the symmetric-nozzle tests were rerun.

The performance of the auxiliary flow channel and the MPMS was highly satisfactory. Pressure-measurement reproducibility over the four scans was within 0.5% at 600-psia supply pressure and within 1% at 100 psia. With no air flowing through the system, atmospheric pressure checks with the instrumentation system proved to be within 1% of measured barometric values.

Some slight variations occurred in the pressures measured by the different taps at a given station. Typical variations in pressure measurements at three axial stations are shown in Fig. 9. All of the pressures at a given axial station fell within a $\pm 1\%$ band about the average pressure measured. This scatter could be attributed to slight variations in orifice axial locations, irregularities in surface geometry, and the pressure-measurement errors previously mentioned.

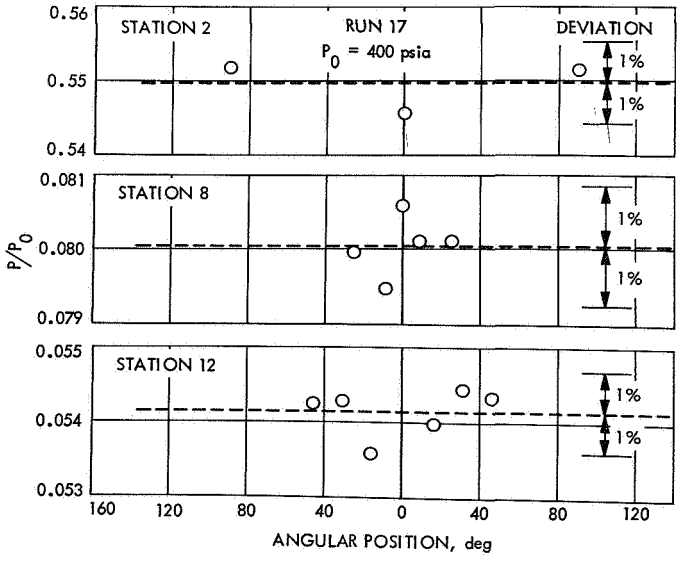

Fig. 9. Wall static-pressure ratio vs nozzle angular position, symmetric nozzle

In Fig. 10, the axial pressure P, ratioed by the plenum-chamber pressure P_0, for a pressure of 400 psia is compared with a one-dimensional isentropic-flow calculation for the symmetric nozzle. The pressure data are averages from the four scans of each pressure orifice.

B. Symmetric Nozzle With Protrusion

Figure 11 shows the ratioed axial-pressure data along the pressure tap centerline with and without the protrusion in place. The ratioed pressure data were found to be essentially independent of supply pressure. An approximate representation of the pressure disturbance produced by the protrusion is given in the contour-pressure plot of Fig. 12. The contour-pressure curves are drawn for various values of the perturbed–unperturbed pressure ratio (P_p/P_u). Data points were obtained by calculating the quotient $(P_p/P_0)/(P_u/P_0)$, and the contours were drawn assuming symmetry about the pressure-orifice centerline. Figure 13 shows axial profiles of the perturbed–unperturbed pressure ratio at cross sections spaced 0, 10, 20, 30, and 40 deg from the pressure-orifice centerline.

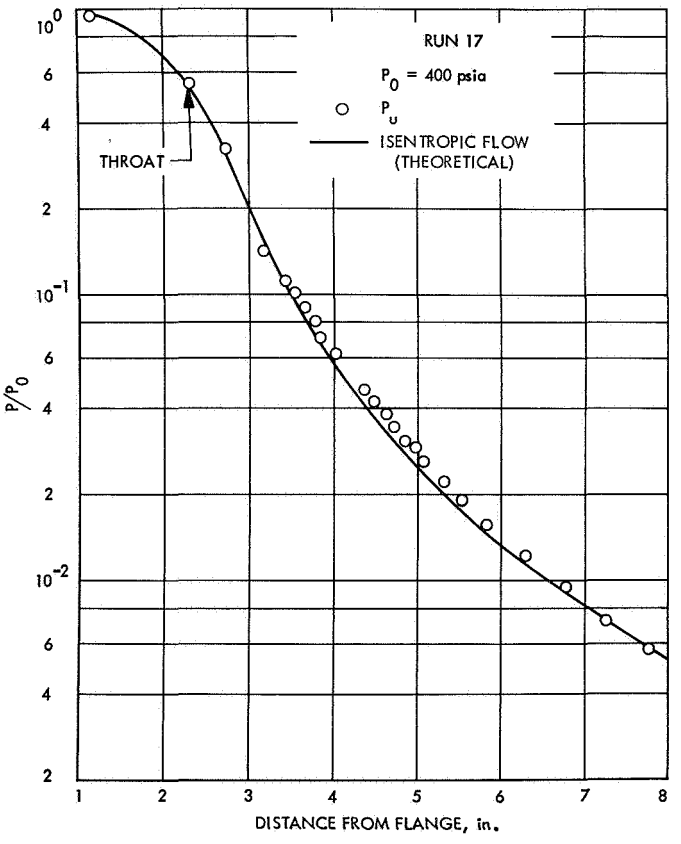

Fig. 10. Measured and theoretical wall static-pressure ratios vs nozzle axial distance, symmetric nozzle

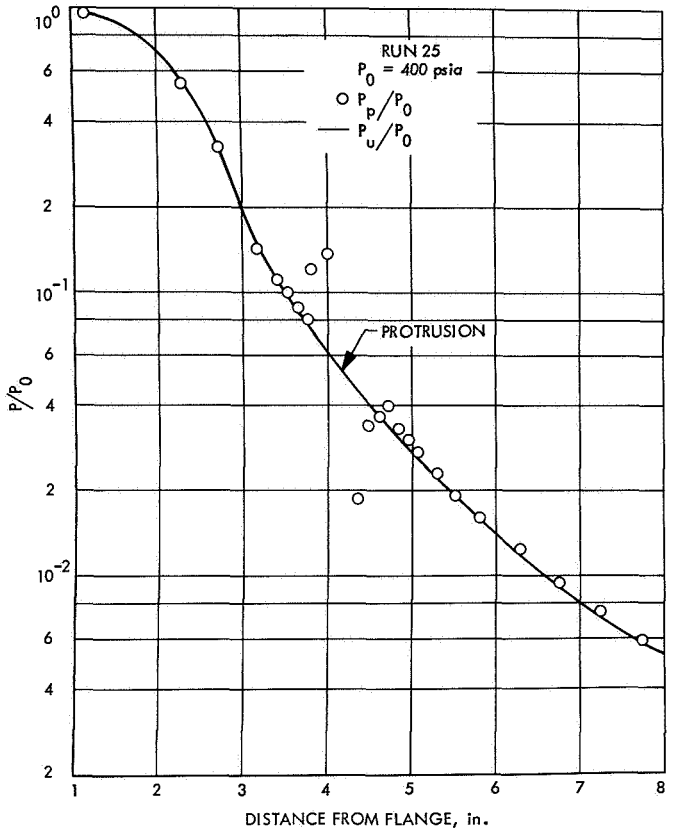

Fig. 11. Perturbed–unperturbed wall static-pressure ratios vs nozzle axial distance, symmetric nozzle

C. Asymmetric Nozzle

In Fig. 14, the ratioed axial-pressure data for a supply pressure of 600 psia are shown for the two angular positions designated in Fig. 6. The circumferential-pressure-ratio profiles at the various axial stations for the asymmetric nozzle are shown in Fig. 15, the angular-position and axial-station designation shown in Fig. 6 again being used. As for the previous data, these pressure-ratio profiles are all independent of the supply pressure.

IV. Side Force Calculations

The net side forces for each of the two nozzles were determined by summing the side force along the cross sections shown in Figs. 3 and 6 over the nozzle expansion ratio ϵ. Results for the symmetric nozzle with protrusion and the asymmetric nozzle are shown in Figs. 16 and 17. The summed net side forces were calculated as ratios of the supply pressures, the two curves thereby describing all test results for each nozzle. The calculated overall net side force for the asymmetric nozzle was slightly under 2% of the nozzle theoretical axial thrust. In Figs. 16 and 17, the force profile reaches a maximum and continues to decrease as the nozzle is traversed along its axis. These maximums are due to changing pressure profiles along the nozzle axes for perturbed and asymmetric nozzles, and will be shown to be not solely attributable to the particular geometries of the test nozzles.

V. Data Analysis

A. Symmetric Nozzle

The measured pressure-ratio data of Fig. 10 fall very close to the one-dimensional, isentropic-flow theoretical curve, being slightly above the curve throughout most of the exit cone. Back, Massier, and Gier (Ref. 2) found data for air at 520°R in the throat region to fall below the one-dimensional, isentropic curve for 15-deg exit cone; however, their data were for nozzles with an $r_e/r_t = 2.00$, whereas the present data are for air flow at ≈560°R in a nozzle with a 15-deg exit cone and an $r_e/r_t = 4.91$. Ahlberg and his associates (Ref. 3) found data that fell above the theoretical curve throughout most of the exit cone. The deviations from the theoretical curve are believed due primarily to deviations from one-dimensional flow, etc.

B. Symmetric Nozzle With Protrusion

A recent review and analysis of the literature concerning turbulent boundary-layer separation in front of a forward-facing step has been published (Ref. 4). The review was restricted to two-dimensional flows in the supersonic-flow range. The following is a summary of the results:

(1) For step heights greater than the boundary-layer thickness, the perturbed-pressure profile is independent of Reynolds number for the small Reynolds number range for which data are available.

(2) The pressure profile is a rather sensitive function of the ratio of step height to boundary-layer thickness (h/δ), when $h < \delta$; but the pressure profile appears to become independent of h/δ for $h > \delta$.

(3) The characteristic physical dimensions of the pressure profile, when normalized by the step height, are roughly independent of Mach number. The pressure rise levels are a function of Mach number.

(4) The induced side force due to the separation ahead of the step, normalized by the ambient pressure and the step height, is approximately a linear function of Mach number.

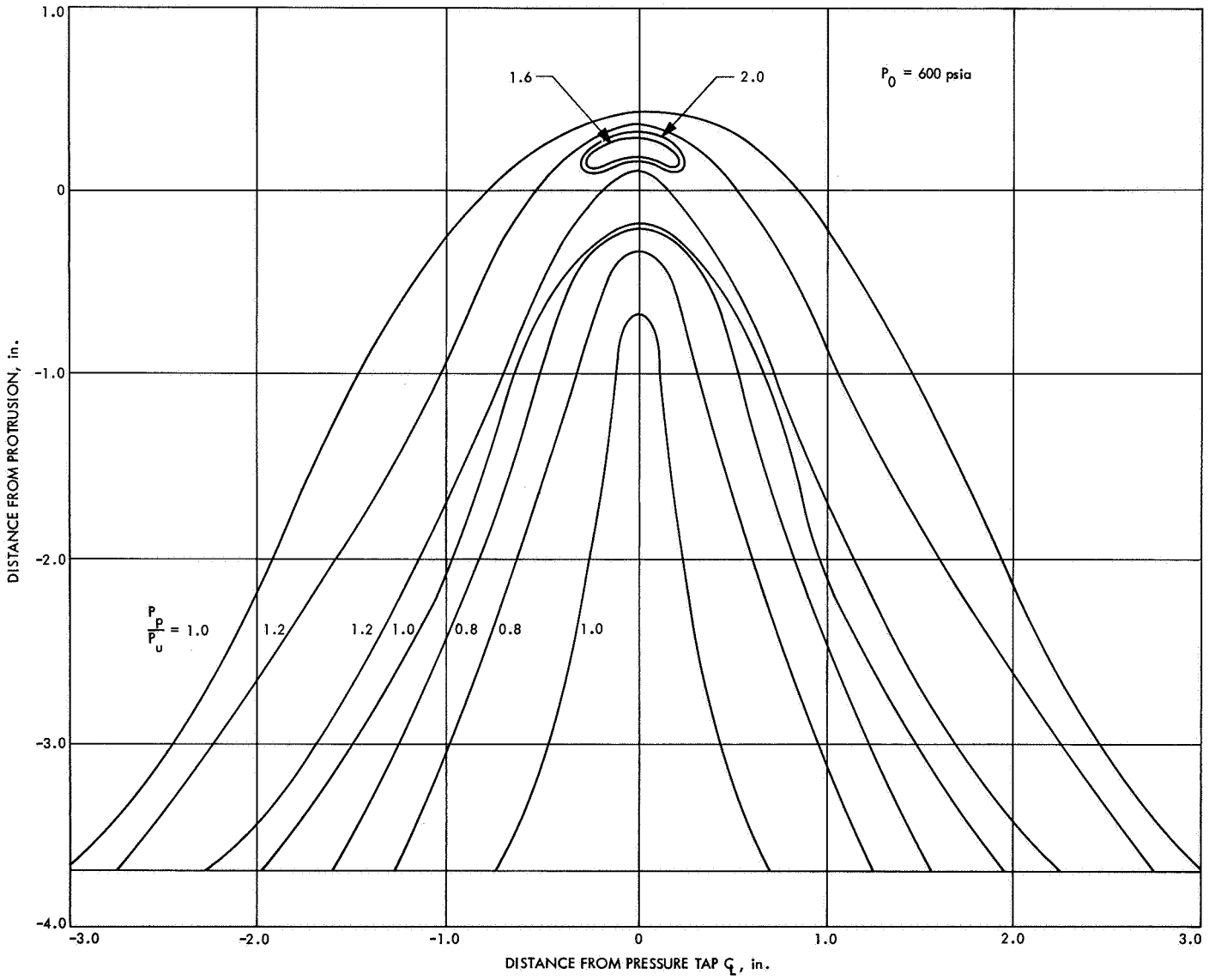

Fig. 12. Contour–pressure plot of disturbance produced by symmetric nozzle protrusion

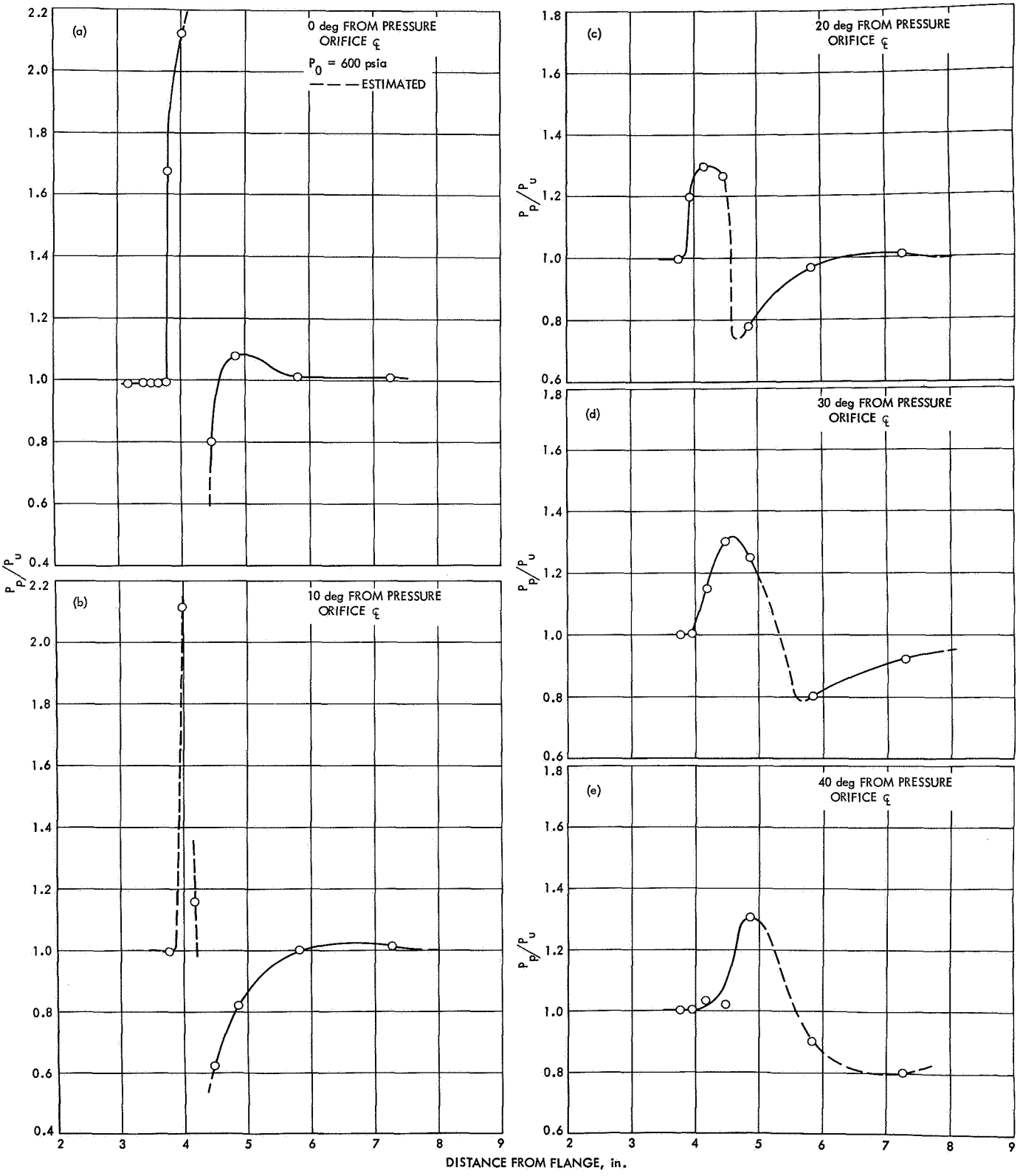

Fig. 13. Perturbed–unperturbed wall static-pressure ratio vs nozzle axial position, symmetric nozzle

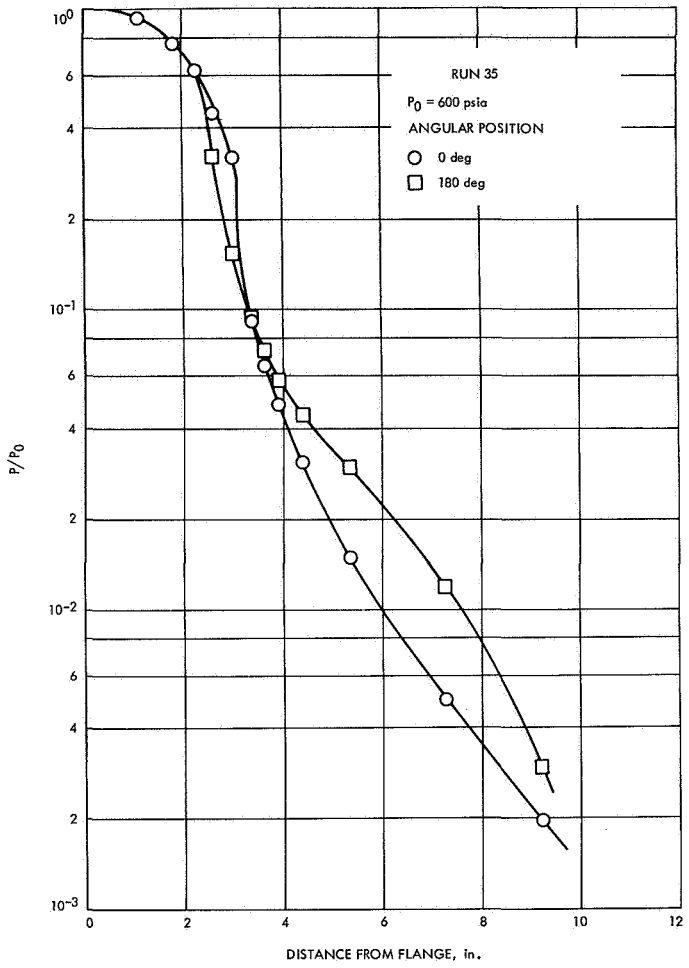

Fig. 14. Wall static-pressure ratio vs nozzle axial distance, asymmetric nozzle

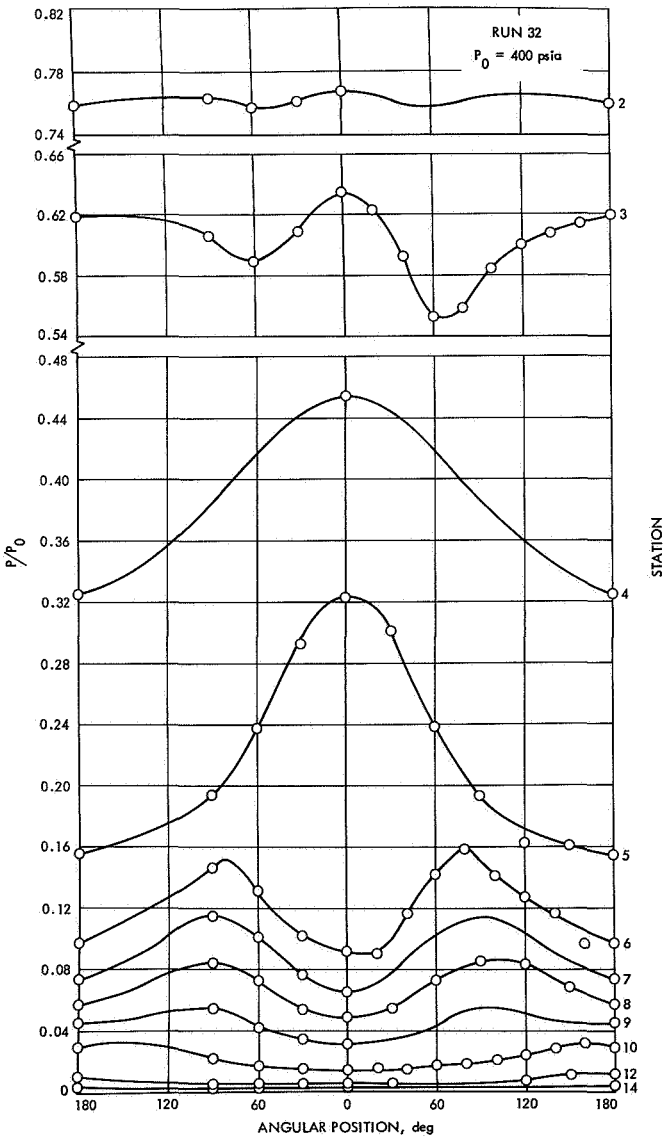

Fig. 15. Wall static-pressure ratio vs nozzle angular position, asymmetric nozzle

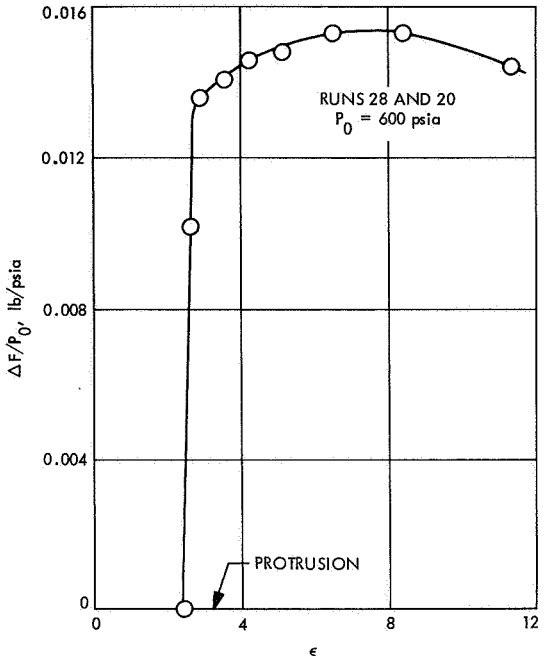

Fig. 16. Summed net side-force/supply-pressure ratio vs nozzle expansion ratio, symmetric nozzle

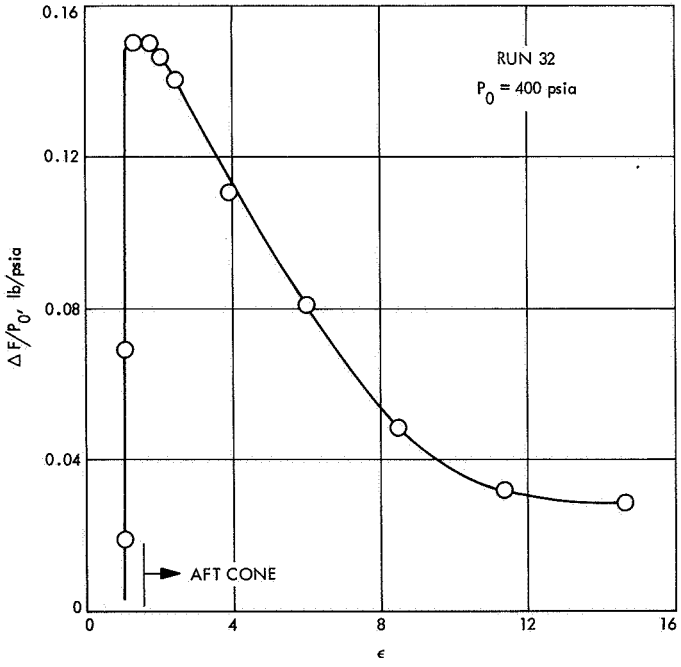

Fig. 17. Summed net side-force/supply-pressure ratio vs nozzle expansion ratio, asymmetric nozzle

The pressure-orifice centerline data of Fig. 13 are replotted in Fig. 18, with a new abscissa of displacement distance along the nozzle surface normalized by the protrusion height, and with the origin set at the forward face of the protrusion. The ambient Mach number at the origin—found from the measured static pressure and one-dimensional, isentropic-flow gas tables—is approximately 2.6. The boundary-layer flow is turbulent (diameter-based Reynolds number greater than 10^6), and the protrusion height is much greater than the value of the velocity boundary-layer thickness calculated at the protrusion location of 0.025 in.

From Fig. 18, the separation distance (normalized by h) is approximately 1.6, and the normalized separation pressure is approximately 1.5. The experimental separation distance is less than half of the predicted values for two-dimensional steps from Ref. 4, whereas the separation pressure is in the predicted region. The maximum value of the integrated side force from Fig. 16, when normalized according to Ref. 4, is approximately 3% of the value predicted because of the separation ahead of the step.

The disparity is due to the fact that, as can be seen from Fig. 13, the flow about the protrusion was highly three-dimensional, with lateral flow around the protrusion exerting a dominating effect. In Ref. 4, it is concluded that, as the lateral flow increases, the separation distance will decrease, the stagnation-point pressure will increase, and the induced side force will decrease, in qualitative parity with the results of this test.

C. Asymmetric Nozzle

1. Two-dimensional nozzle flow-field analyses. A three-dimensional, method-of-characteristics solution for the flow field in the asymmetric nozzle, although possible,

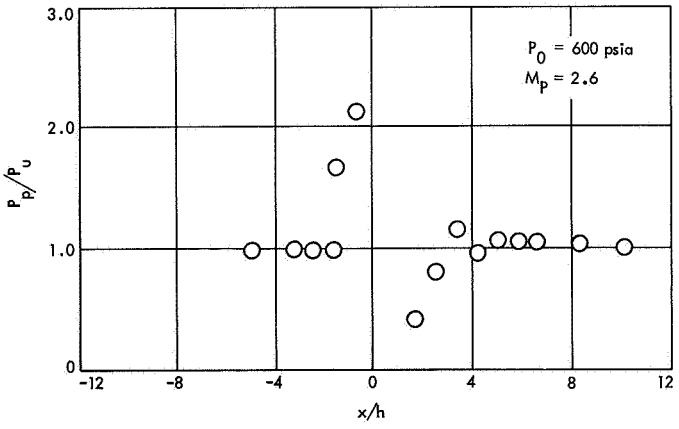

Fig. 18. Perturbed–unperturbed wall static-pressure ratio along pressure-orifice centerline vs nondimensionalized displacement distance from protrusion forward face

would be very tedious and time-consuming. Also, a solution for the sonic surface would be difficult to obtain. To get some feeling for the pressure distributions that might be expected, a semigraphical method-of-characteristics flow-field hand calculation was carried out for a two-dimensional nozzle, designated Nozzle A (Fig. 19), having the same wall profile as the asymmetric nozzle in a nozzle cross-sectional plane along the major axis of the ellipse. The transition corners (points 1 and 2 in Fig. 19) were assumed sharp for the two-dimensional nozzle, necessitating the use of Prandtl–Meyer corner-flow expansions in the calculated pressure-ratio profiles. In the actual nozzle, these transition regions were slightly rounded.

The origin of the coordinate system was located at the center of the geometric throat, as shown in Fig. 19. The approximate shape of the sonic line for the two-dimensional nozzle was obtained using the method given by Hall (Ref. 5) with modified boundary conditions. This calculation resulted in the following equation for the sonic line:

$$x^* = 0.086 - 0.516y^* - 0.258y^{*2} \qquad (1)$$

Because the starting line for a method-of-characteristics solution must be supersonic ($M > 1$), the following equation for the $M = 1.15$ line was obtained:

$$x = 0.474 - 0.516y - 0.258y^2 \qquad (2)$$

Using the $M = 1.15$ line as the starting line, a method-of-characteristics solution for nozzle A was obtained. The wall-pressure profiles from the method-of-characteristics solution were compared with the asymmetric-test-nozzle results in Fig. 20. The comparison showed the expected differences between the pressure profiles for the two- and three-dimensional nozzles. The greater area expansion with increased axial distance of the three-dimensional nozzle was accompanied by a more rapid pressure expansion, although the trends of the set of wall-pressure profiles for each of the two nozzles were the same. The flow along the lower wall of each nozzle expanded more slowly than the flow along the upper wall until the sudden expansion into the aft cone region occurred (point 2 in Fig. 19), where the two pressure profiles crossed.

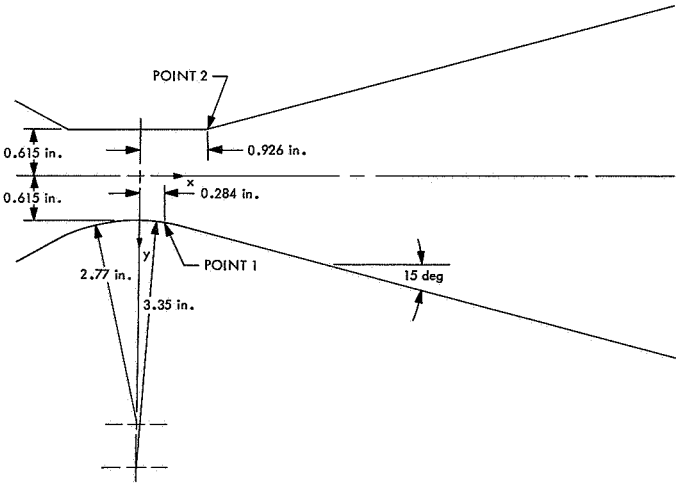

Fig. 19. Nozzle A

When considering the side force that might be produced in nozzle A, it is apparent that the crossing of the two wall static-pressure profiles in Fig. 20 will tend to have a canceling effect on the net side force. This canceling effect might be caused by the particular geometry of the wall profile, and might be missing in an asymmetric nozzle with smooth wall profiles. To examine this possibility, a method-of-characteristics solution was obtained for the two-dimensional asymmetric nozzle (nozzle B in Fig. 21).

The wall-pressure profiles from the method-of-characteristics solutions for nozzles A and B are compared in Fig. 22. The wall-pressure profiles for nozzle B are very similar to those for nozzle A, except that the pressure difference between the two walls is less and the sharp Prandtl–Meyer pressure expansions are absent.

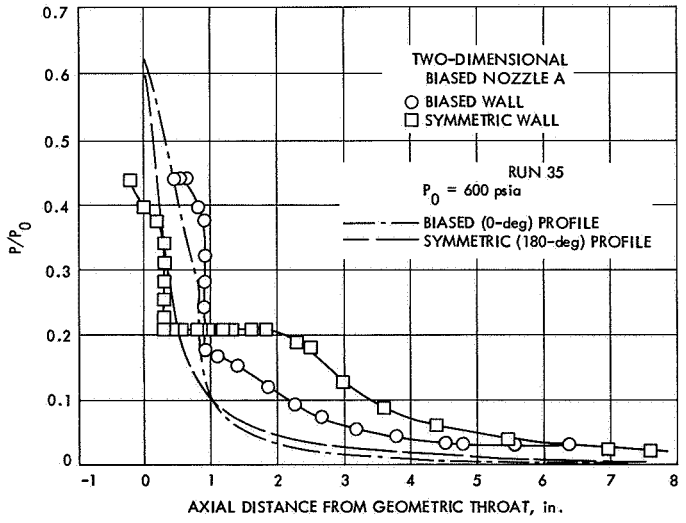

Fig. 20. Comparison of method-of-characteristics static-pressure ratio profiles for nozzle A with asymmetric nozzle test results

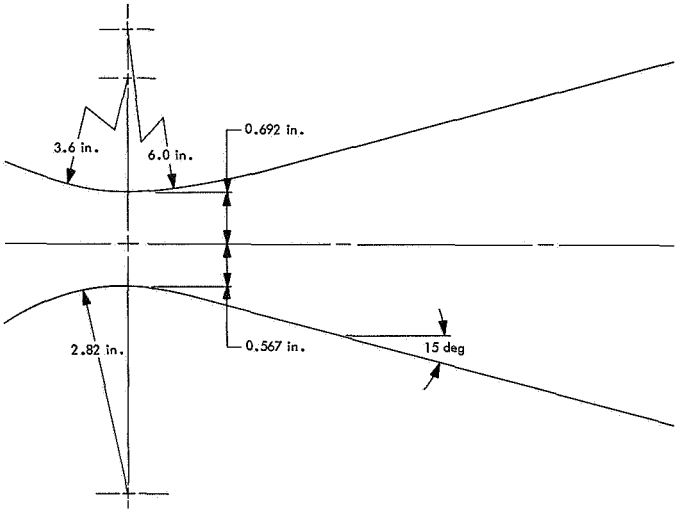

Fig. 21. Nozzle B

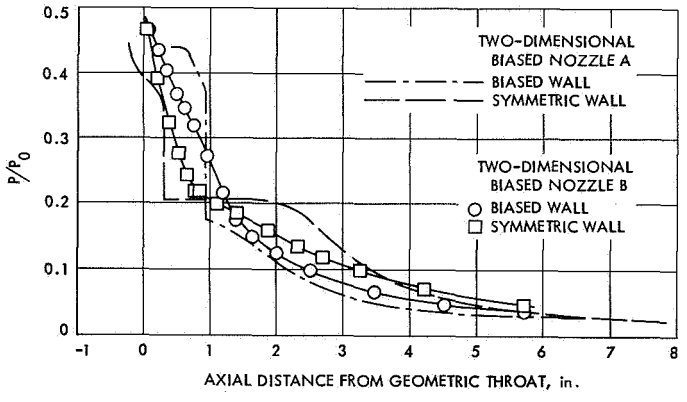

Fig. 22. Comparison of method-of-characteristics static-pressure ratio profiles for nozzles A and B

Considering the side forces produced, the canceling effect of the two wall-pressure profiles is therefore still present, even for an asymmetric nozzle with smooth wall profiles.

2. Three-dimensional nozzle flow-field analysis. Some simple calculations were made to get a qualitative picture of the flow through the three-dimensional asymmetric nozzle. An approximate shape for the sonic surface of the asymmetric nozzle was calculated using the equations developed for axisymmetric flow by Shapiro (Ref. 6). The coordinate system was located as shown in Fig. 23. A hypothetical axisymmetric nozzle was considered with a throat radius of 1.231 in. and a throat radius of curvature of 2.77 in. with the centerline located on the X-axis. The throat radius of curvature upstream of the geometric throat was used because it influences the

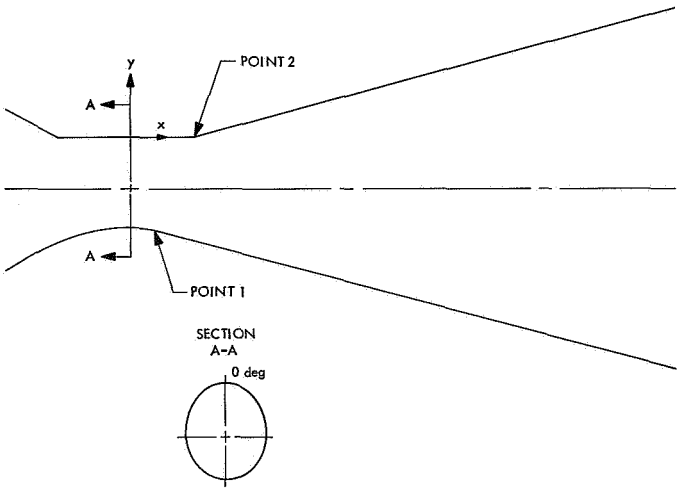

Fig. 23. Coordinate system for three-dimensional nozzle flow-field analysis

subsonic flow as the flow approaches sonic speed (and it is thus the proper choice for calculating the sonic surface). The equation for the sonic line in the hypothetical axisymmetric nozzle is given by

$$x^* = 0.225 - 0.297y^* \tag{3}$$

Equation (3) was assumed to represent the sonic line in the asymmetric nozzle. The actual throat in the asymmetric nozzle would be expected to shift downstream because of the combination of boundary-layer effects and small variation of the nozzle area with displacement of x in the throat region. Because of the uncertainty in actual throat location, the sonic line given by Eq. (3) was shifted downstream by 0.255 in. to permit matching of the calculated peak pressure in the pressure profile at station 5 with the experimental peak pressure at the same station (see Fig. 15). A determination of the sonic points on the wall of the asymmetric nozzle was made by determining the intersection of Eq. (3) with the inner surface of the asymmetric nozzle.

The flow deflection angles at the two corners (points 1 and 2) were calculated as a function of the angular position in the nozzle; these angles are shown in Fig. 24. To obtain the circumferential pressure profile at an axial station downstream of the sonic surface, the calculation was divided into two separate parts. First, the pressure profiles were calculated assuming no angular variation of the profiles as they expanded out the nozzle. Second, the change in position of the pressure peaks in the profiles with expansion of the flow was calculated.

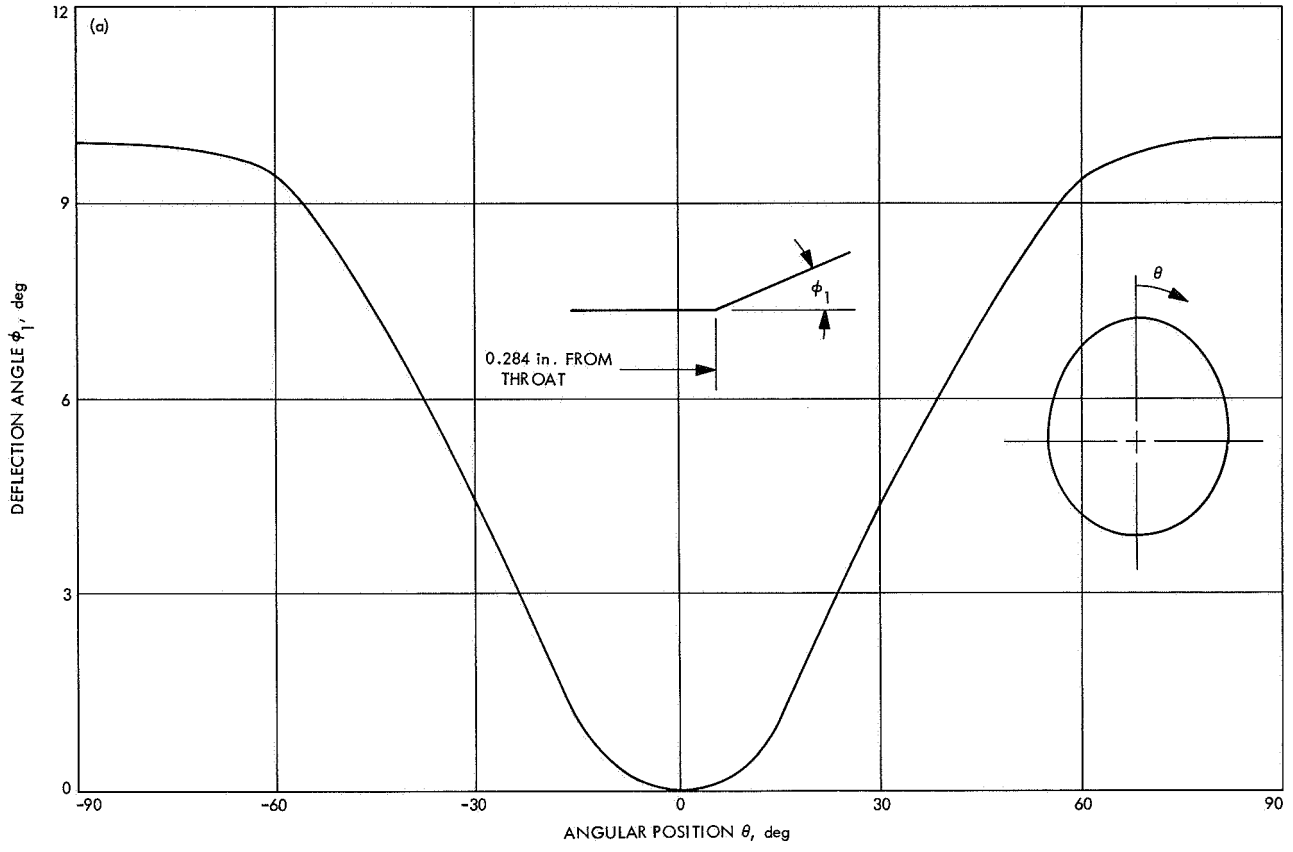

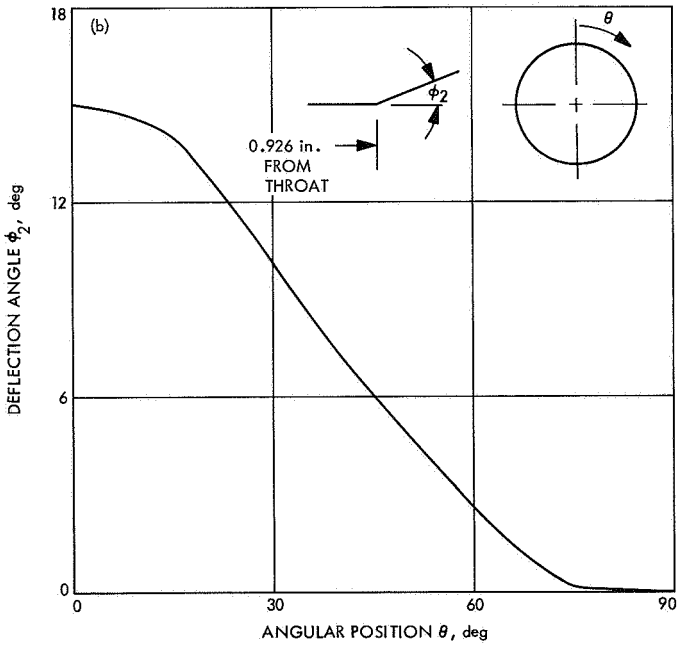

Fig. 24. Flow deflection angle as a function of nozzle angular position: (a) corner 1, (b) corner 2

The first calculation started with the conditions at the wall sonic line and used a local point-by-point isentropic axial expansion, except at points 1 and 2, where a Prandtl–Meyers expansion through the local flow deflection angle in Fig. 24 was used.

For the second calculation, it was observed that downstream of point 2 the circumferential pressure profile assumed a shape of two pressure waves. It was assumed that such pressure waves propagate downstream on the surfaces of the local Mach cones. Taking the intersection of the local Mach cone with the nozzle wall, the propagation of these pressure waves along the nozzle wall was determined. Pressure profiles calculated in this manner were compared with the experimentally observed profiles in Fig. 25, plotting in the same manner as Fig. 15. Agreement, for a simplified calculation such as this, is considered reasonably good.

VI. Two-Dimensional Asymmetric-Nozzle Parametric Study

A. Introduction

The problem remains of attempting to extend the asymmetric nozzle experimental results to nozzle conditions of reduced asymmetry, more in line with the magnitudes of asymmetry that can occur in actual rocket nozzles (erosive increase in the nozzle-throat radii of several ten-thousandths of an inch). To assist in the solution of this problem, a computer program was developed that enables the flow characteristics for a nozzle with any degree of asymmetry to be determined. The decision was made to limit the analysis to two-dimensional nozzles, as the complexity of a three-dimensional asymmetric program would be prohibitive. An attempt would be made to relate the calculated results to the three-dimensional case, using the existing experimental information.

B. Nozzle-Flow Analysis Computer Program

Use was made of a Boeing Scientific Research Laboratory method-of-characteristics computer program (Ref. 7) for the analysis of two-dimensional or axially symmetric, isentropic or variable-entropy nozzle flow of a perfect gas in the supersonic region. This program was modified to analyze two-dimensional asymmetric nozzles with prescribed upper and lower wall boundaries. Each boundary consisted of a circular arc of radius R and a conical section with a half-angle α. The program can use either an input initial Mach line (>1) or calculate a uniform

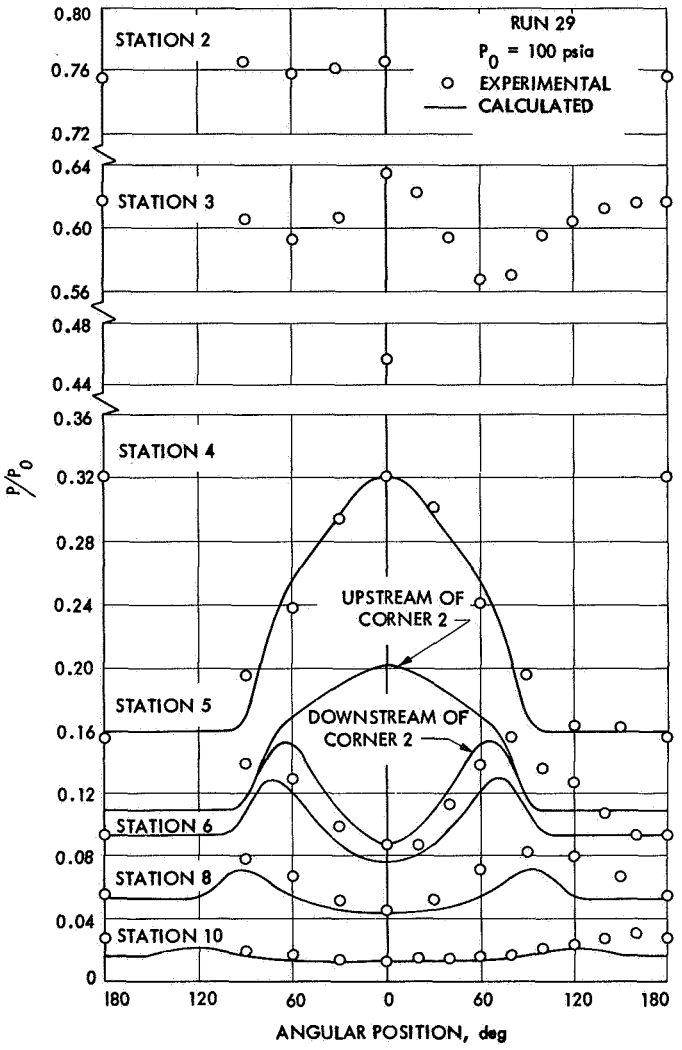

Fig. 25. Comparison of calculated circumferential static-pressure ratio profiles with asymmetric-nozzle test results

starting line of M prescribed points using uniform spacing between the defined boundaries. Printed outputs consist of: (1) the coordinate, pressure ratio, Mach number, and entropy at each point where a Mach line intersects a boundary, or (2) this information, excluding pressure ratio, printed for each point of the characteristic net. A plot of pressure ratio vs axial coordinate is generated for both the upper and lower boundaries.

C. Program Calculations

Using the computer program, the boundary pressure data for a family of two-dimensional nozzles of increasing asymmetry (Fig. 26) were calculated. The configuration variables were the distances from the nozzle centerline to the lower and upper boundaries at the nozzle throat (r_1 and r_2), the difference divided by 2

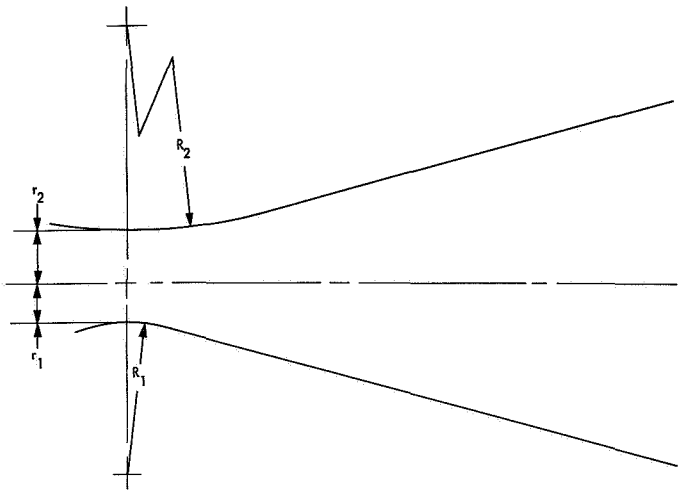

Fig. 26. Two-dimensional asymmetric nozzles

being the throat asymmetry, and the radii of curvature of the circular portion of the lower and upper boundaries (R_1 and R_2). Calculations were run for the seven cases listed in Table 1.

Table 1. Nozzle dimensional data for determination of boundary pressure calculations

Case[a]	r_2, in.	R_2, in.	$(r_2 - r_1)/2$, in.
1	0.526	2.04	0
2	0.538	2.38	0.006
3	0.550	2.72	0.012
4	0.575	3.42	0.025
5	0.600	4.13	0.037
6	0.650	5.55	0.062
7	0.705	7.11	0.090

[a]In all cases, $r_1 = 0.526$ in. and $R_1 = 2.04$ in.

The values for R_1 and r_1 were held fixed for all seven cases, but R_2 and r_2 were increased from the case 1 values of R_1 and r_1 (symmetric nozzle) to the case 7 maximum values. A conical half-angle of 15 deg was used. The r_1 and r_2 values for the case 7 configuration were the same as those of the three-dimensional asymmetric test nozzle.

Preliminary calculations were made to compare the nozzle-pressure ratios computed using the two possible starting Mach line inputs: first, a modified version of the Sauer transonic flow solution and, second, a uniform starting line. The agreement was considered adequate for qualitative-trend calculations; therefore, the second starting Mach line procedure was used for all calculations.

D. Calculation Results

The surface-pressure ratios at the nozzle boundary were calculated for the seven 2-dimensional nozzle cases, and are shown in Fig. 27. The increasing divergence of the pressure profiles for the two boundaries with increasing nozzle asymmetry is evident. The measured cross-sectional, static-pressure-ratio data for the asymmetric test nozzle are shown again in Fig. 28 for comparison purposes.

The net side force normal to the nozzle axis was calculated for each of the two-dimensional nozzle cases by numerically integrating the calculated pressure distributions over the two boundaries of each nozzle. A nozzle width of unity was used to simplify the calculations. The resulting side-force axial profiles (presented as the net side-force-to-axial-thrust ratio summed over the nozzle expansion ratio) for the seven nozzle cases are shown in Fig. 29. Nozzle axial thrust was calculated, assuming one-dimensional isentropic flow and neglecting the nozzle-exit, ambient-pressure differential term.

An oscillatory type of side-force axial profile was obtained for each of the calculated cases. The summed net side-force ratio reached a maximum value, reversed itself at the point where the two pressure-ratio profiles crossed, crossed the abscissa and reversed its direction, and finally leveled off at the overall value for the nozzle. The peak and overall side-force values (amplitudes of the side-force axial profile) decreased with decreasing nozzle asymmetry. The crossover at the abscissa occurred at nozzle ϵ values of 2 to 2.5 in. (axial distances of 2–4 in. from the geometric throat). The overall side-force values decreased from a maximum of 2.25% of the theoretical axial thrust to a value of approximately 0.75% for the minimum asymmetry case (case 2).

Writing the expression used to calculate the two-dimensional nozzle side-force-to-axial-thrust ratio at an expansion ratio ϵ:

$$\left(\frac{\Delta F}{T}\right)_\epsilon = \frac{\sum_{i=1}^{\epsilon}\left[\Delta A\left(\frac{P}{P_0}\right) f(\phi)\right]_i}{M_\epsilon A^* \gamma\left[\left(\frac{2}{\gamma+1}\right)^{\frac{\gamma+1}{\gamma-1}}\right]^{1/2}\left[\frac{1}{\left(1+\frac{\gamma-1}{2}M_\epsilon^2\right)^{1/2}}\right]^{1/2}} \tag{4}$$

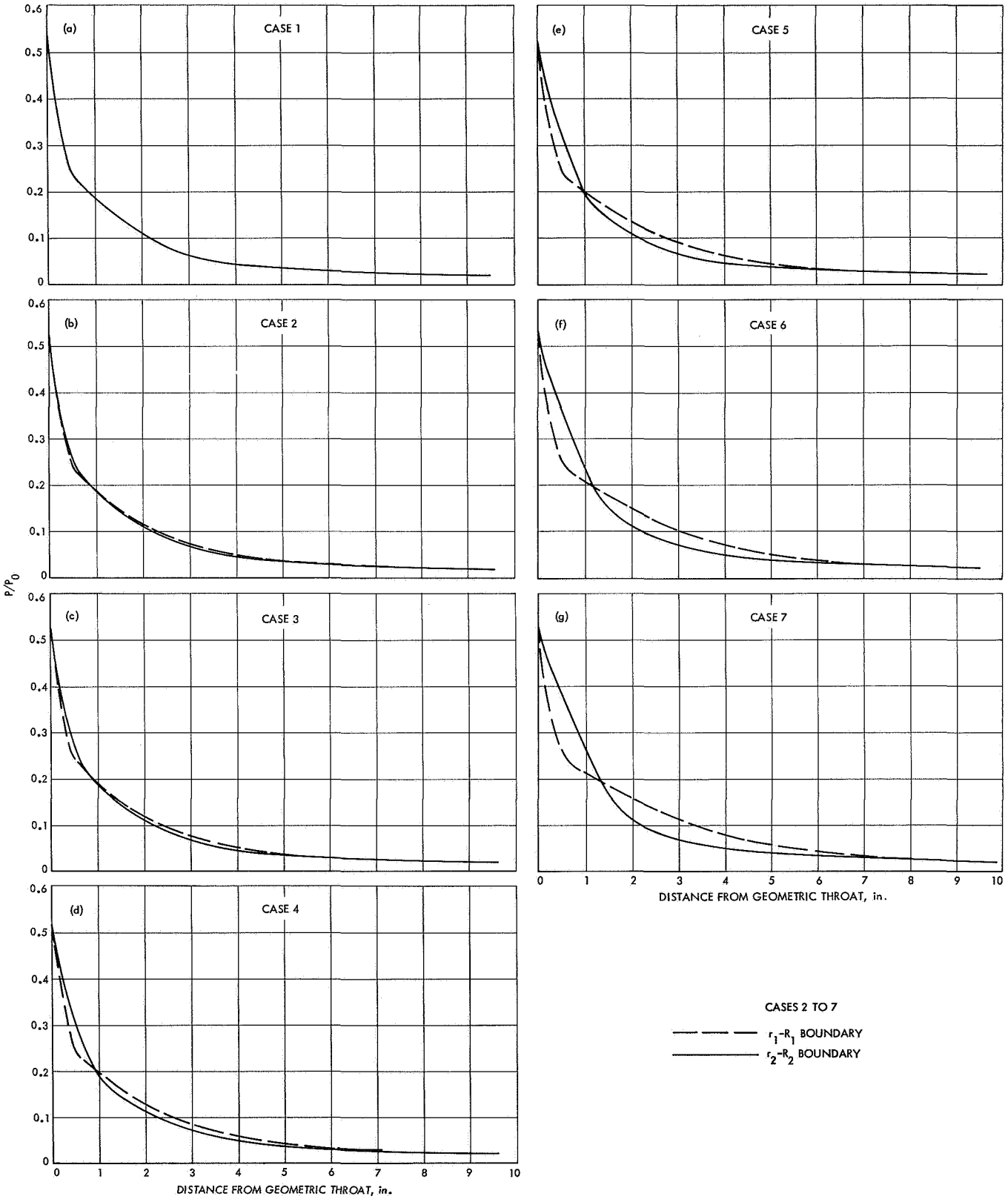

Fig. 27. Calculated wall static-pressure ratio vs nozzle axial distance: (a) case 1, (b) case 2, (c) case 3, (d) case 4, (e) case 5, (f) case 6, and (g) case 7

Defining and reducing terms:

ΔA_i = nozzle surface area element

$\propto r_t$ in the throat region (for r_c/r_t = constant)

= constant in aft conical section

$P/P_0 \approx f(\epsilon)$

ϕ = vector direction of area segment with respect to nozzle axis

= nozzle expansion angle in aft conical section

M_ϵ = Mach number

$= f(\epsilon)$

A^* = sonic throat area

$\propto r_t$

γ = ratio of specific heats

Substituting for the terms in Eq. (4), the r_t terms cancel, and to a good approximation, $(\Delta F/T)_\epsilon$ is a function only of ϵ and γ for geometrically similar nozzles.

E. Discussion

Because of the differing nozzle expansion characteristics for two- and three-dimensional nozzles (Section V-C-1), the calculated results obviously cannot be directly related to actual three-dimensional nozzle conditions, but certain trends and predictions can be determined.

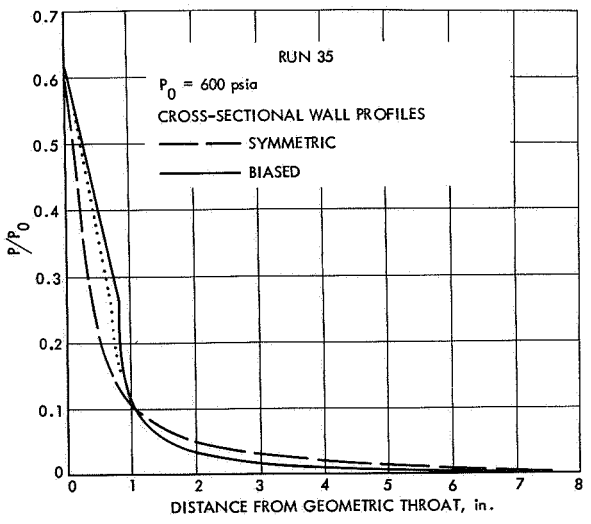

Fig. 28. Measured wall static-pressure ratio vs nozzle axial distance, asymmetric nozzle

For the experimental nozzle (see Fig. 17), the side-force axial profile leveled off at a positive value, never crossing the abscissa. A nozzle with a smoother, less abrupt throat-region contour (similar to two-dimensional nozzle contours used), but with the same degree of asymmetry, would be expected to produce a smoother, less abrupt pressure expansion along the biased wall portion of the nozzle throat, as illustrated by the broken line in Fig. 28. This would result in a reduced maximum net side-force value and an overall value that approaches zero and probably crosses the abscissa, reversing the direction of force.

Based upon this interpretation of the experimental results, the effect of reduced magnitude of asymmetry on the net side-force characteristics for three-dimensional nozzles is predicted to be qualitatively the same as for the two-dimensional calculated results—a reduction in the amplitudes of an oscillatory type of net side-force axial profile. The overall nozzle side force should be less than 1% of the nozzle axial thrust (0.5 deg of misalignment in the thrust vector) for the magnitudes of nozzle-throat asymmetry found in actual rocket nozzles.

The theoretical analysis contained in a recent paper on this subject (Ref. 8) also predicts an oscillatory type of side-force axial profile as a result of asymmetric flow in the throat region of a rocket nozzle. The paper also reports the results of some static-firing experiments that are in general agreement with the preceding conclusions.

Small rockets with nozzles with known asymmetries were static-fired in a six-component test stand. A reported curve of lateral-force-to-axial-thrust ratio vs nozzle length exhibited the oscillatory form, with an amplitude of 0.5%.

VII. Summary and Conclusions

The following statements briefly summarize the results of this program:

(1) For both nozzles, all pressure data ratioed by the plenum supply pressure P_0 were essentially independent of test supply pressure.

(2) For both nozzles, the net side force, summed over the nozzle expansion ratio, reached a maximum, then continued to decrease as the nozzle was traversed along its axis, leveling off at a minimum overall value for the asymmetric nozzle case.

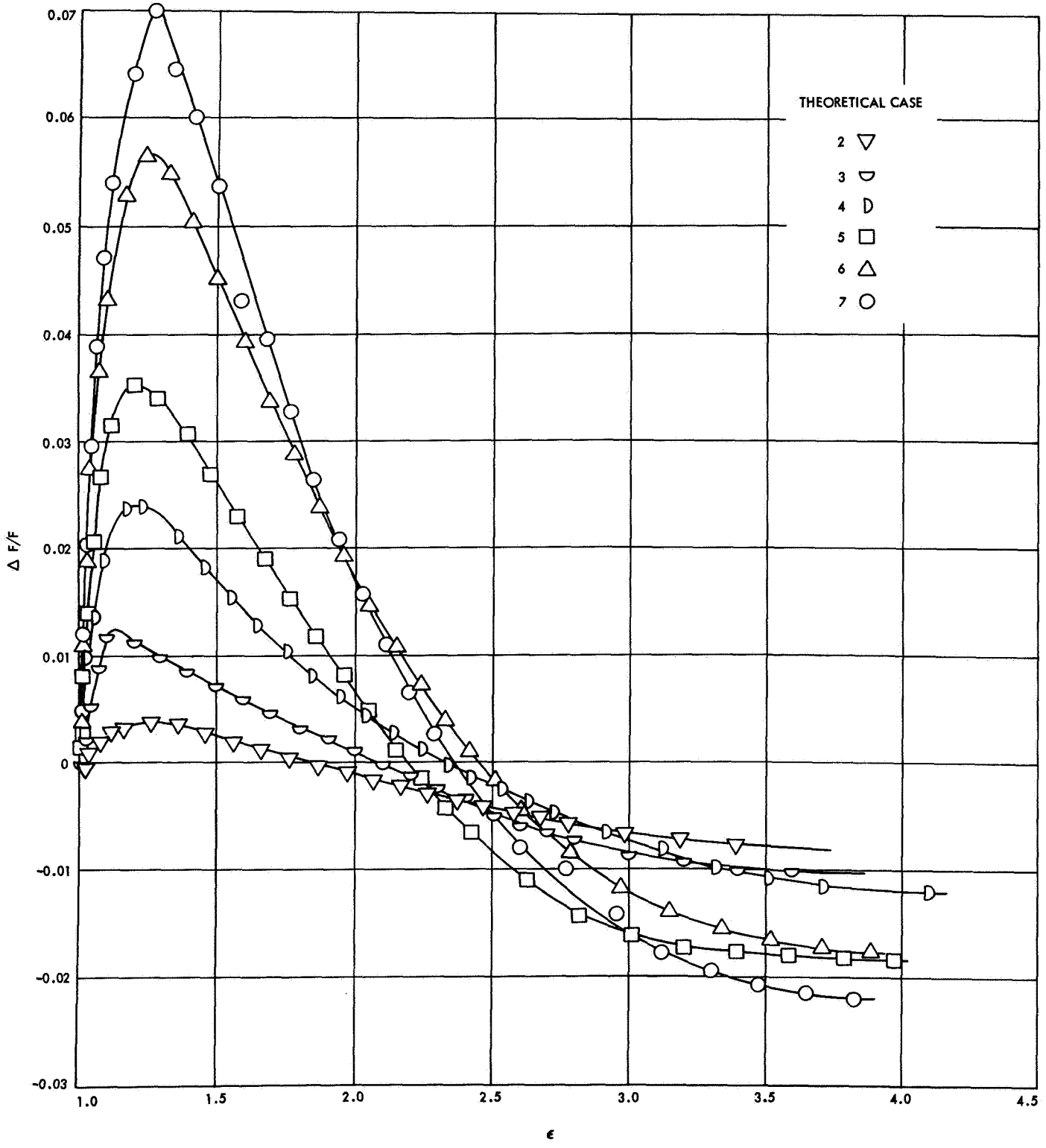

Fig. 29. Summed net side-force/axial-thrust ratio vs nozzle-expansion ratio, two-dimensional asymmetric nozzles

(3) The characteristics of the perturbed–unperturbed pressure-ratio profile approached those of pressure-ratio profiles found by other investigators for flat-plate, turbulent-boundary-layer flow over two-dimensional protrusions, the differences, in all probability, being due to the three-dimensional nature of the experimental protrusion.

(4) The asymmetric nozzle net side-force profile maximum was determined to be not solely attributable to the particular geometry of the test nozzle.

(5) A highly simplified three-dimensional flow-field analysis gave reasonably good parity with the asymmetric-nozzle experimental data.

(6) A two-dimensional asymmetric nozzle parametric analysis predicts, it is believed, the correct trend of change in magnitude of induced nozzle side force with decreasing degree of throat asymmetry.

It is concluded that nozzle-surface irregularities and throat asymmetry can produce measurable and possibly significant side forces. Using mean values of the localized static pressure and Mach number, scaling laws for flat-plate supersonic flow over a protrusion can be applied to irregularities in the nozzle expansion cone to obtain an approximate indication of the perturbed-pressure profiles and, therefore, the induced side forces.

Asymmetry in the region of the nozzle throat will produce an oscillatory type of net side-force axial profile.

To obtain a first estimate of the induced side force, it is recommended that a rough surface-pressure integration be carried out using axial-pressure profiles obtained by a two-dimensional flow analysis in the plane of the desired side-force direction.

References

1. Strand, L. D., Newton, J. F., Jr., and Herrera, J. G., *Initial Performance of a New Nozzle Gas-Dynamics Test Facility,* Technical Memorandum 33-310. Jet Propulsion Laboratory, Pasadena, Calif., Nov. 15, 1966.
2. Back, L. H., Massier, P. F., and Gier, H. L., *Comparisons of Experimental With Predicted Wall Static-Pressure Distributions in Conical Supersonic Nozzles,* Technical Report 32-654. Jet Propulsion Laboratory, Pasadena, Calif., Oct. 15, 1965. (Also appears in *AIAA J.*, Vol. 3, No. 9, pp. 1606–1614, Sept. 1965.)
3. Ahlberg, J. H., et al., "Truncated Perfect Nozzles in Optimum Nozzle Design," *ARS J.*, Vol. 31, pp. 614–620, 1961.
4. Zukoski, E. E., "Turbulent Boundary-Layer Separation in Front of a Forward-Facing Step," *AIAA J.*, Vol. 5, No. 10, pp. 1746–1753, 1967.
5. Hall, I. M., "Transonic Flow in Two-Dimensional and Axially Symmetric Nozzles," *Quart. J. Mech. Appl. Math.*, Vol. 15, pp. 487–508, 1962.
6. Shapiro, A. H., *The Dynamics and Thermodynamics of Compressible Flow: Volume II.* The Ronald Press Company, New York, 1954.
7. Ehlers, F. E., *An IBM 7090 Program for Computing Two-Dimensional and Axially Symmetric Flow of an Ideal Gas,* Mathematical Note 727. Mathematics Research Laboratory, Scientific Research Laboratory D1-82-0204, Boeing Co., Seattle, Wash., Nov. 1962.
8. Darwell, H. M., and Trubridge, G. F. P., "The Design of Rocket Nozzles to Reduce Gas Misalignment," paper presented at the ICRPG/AIAA Second Solid Propulsion Conference, Anaheim, Calif., June 1967. Preprint in bound volume published by the American Institute of Aeronautics and Astronautics, pp. 198–205, New York, 1967.